

Computational Analysis of Serpentine Nozzles



Somrick Das Biswas, Keshav Anand Kabra, Shailesh R. Nikam,
and Siddharth Anish

1 Introduction

Serpentine nozzles completely shield the high-temperature core flow and the tail cone inside the core wall, which indicates that the core walls and the high-temperature parts inside the core wall are invisible from all directions at the rear of the serpentine nozzle.

Recently, serpentine nozzles have attracted considerable attention, especially in military aviation. Serpentine nozzles suppress the thermal and acoustic signatures of the engine exhaust, making the aircraft difficult to track by radars and IR-homing missiles and seekers. In this paper, the main focus is on improving the expansion characteristics to reduce the performance penalty associated with serpentine nozzles. However, little research exists on predicting elementary flow characteristics like pressure and velocity gradients within the nozzle. Furthermore, the effects of inlet and outlet shapes on the flow parameters are not known. The paper aims to infer a relationship between geometry and flow behaviors. The literature survey has proved that serpentine nozzles have excellent stealth characteristics and avoid detection. As stealth becomes a primary consideration in future wars, the significant thrust penalties are the tradeoffs for operating in hostile airspace.

S. Das Biswas (✉) · K. A. Kabra · S. Anish

Department of Mechanical Engineering, K. J. Somaiya College of Engineering, University of Mumbai, Mumbai, India

e-mail: somrick.d@somaiya.edu

K. A. Kabra

e-mail: keshav.kabra@somaiya.edu

S. Anish

e-mail: siddharth.anish@somaiya.edu

S. R. Nikam

Department of Mechanical Engineering, K. J. Somaiya College of Engineering, Somaiya Vidyavihar University, Mumbai, India

2 Literature Review and Objective

Several research papers were consulted and studied during the literature study phase to gain a deeper understanding of the topic. The different research papers consulted for this paper are summarized below.

Hui et al. [1] investigated the serpentine nozzle experimentally and computationally. They studied flow characteristics of serpentine nozzles and axisymmetric nozzles with the employment of a schlieren system, PSI electronic pressure scanning valves, a six-component force balance system, and flowmeters. Their results show that the static pressure distributions on the upper and down walls of serpentine nozzles are different from those of axisymmetric nozzles, which are mainly affected by the flow tube near the walls. The flow velocity increases and the static pressure drops when the flow tube contracts. This paper serves as the primary basis of our validation.

Cheng et al. [2] found that the shielding ratio has a significant impact on the infrared signature of the serpentine nozzle. The analysis indicates that the serpentine nozzle with $\Delta Y = 1$ has a better stealth performance; additionally, the visible area ratio is suggested to be under 0.041. The swirl angle significantly affected the infrared signature level of the serpentine nozzle. Compared to the no-swirl case, the average reduction of the total infrared signature level increased from 2.29 to 13.84% in the horizontal plane for an increase in the swirl angle from 5° to 20° . An increased reduction from 5.83 to 31.21% is seen in the vertical plane.

Shan et al. [3] had the following findings. The nozzle with an aspect ratio of 5 is recommended for achieving optimal aerodynamics. The increase in aspect and offset ratios could effectively suppress plume radiation, which was not sensitive to overall radiation. Compared with circular nozzles, the double S-shaped nozzles reduced infrared radiation by over 50%, proving significant stealth ability. A balance between aerodynamic performances and infrared radiation suppression could be reached for double S-shaped nozzles.

Nageswara Rao et al. [4] experimentally discussed the effect of the nozzle shape on the flow field and acoustic characteristics of a high Mach no. subsonic jet emanating from a serpentine nozzle at Mach number 0.84. Near-field OASPL mapping results indicate that the dominant noise is emanating at the end of the potential core breakdown.

Sun et al. [5] investigated and surmised that the centerlines with a rapid turning at the exit would result in a high Mach number, which brings on high friction loss and secondary loss at the turnings. For maximum efficiency of centerline distributions, it is recommended that curves with gentle turns at each serpentine passage exit should be chosen.

Da et al. [6] theorized that with a sectional PI control law, the RMS control error was reduced by more than 56% under arbitrary changing conditions. Works in this paper also showed that the dynamics of this non-dimensional system can be simplified as a stable second-order overdamped system.

3 Materials and Methods

In the present investigation, CFD simulations are undertaken using the Ansys Fluent 2021R2 version. The first step was to validate the CFD results from existing literature in [1]. Once an accurate enough model was established to give predictable results, new iterations were undertaken to study the control variables of a serpentine nozzle to derive the optimum geometry.

After a few iterations, the established CFD model could accurately and consistently deliver the expected values. Once the CFD models attained critical stability based on a grid independence study, literature data [1] were compared with our model predictions. This process is highlighted in Fig. 10.

The present results match well within 10% of the literature result with a similar trend and thus helped us gain reasonable confidence in our CFD model.

Post-validation, we decided to focus our attention on the different geometrical parameters of the serpentine nozzles. We have mainly focused on revamping the inlet and outlet geometries and tried multiple iterations such as elliptical, circular, rectangular, and cambered rectangular outlet geometries. These geometries and their CAD models and properties are discussed in the subsequent section.

Following this, pressure and velocity contours of the geometries were studied and investigated to arrive upon the most optimum geometry, which would meet our objectives of reducing thrust penalties, by modulating pressure and velocity flows.

The pressure and velocities contours have been plotted in the nozzle mid-plane. We have attempted to reduce the pressure perturbations to reduce abrupt pressure variations.

The secondary objective is to study the velocity flow lines to ensure maximal exhaust velocity and to produce the highest amount of thrust possible from the engine.

3.1 Nozzle Geometry

The basic profile of the serpentine nozzle is seen in Fig. 1. The serpentine nozzle is modeled using Bezier curves in SolidWorks 2021. Five guide points are used to model the profile.

Several variations in inlet and outlet geometries were simulated, and their characteristics are analyzed. Their specifications are listed as follows:

3.1.1 Cambered Rectangular Exit

See Figs. 2 and 3.

Inlet diameter: 250 mm.

Rectangular exit camber diameter: 100 mm.

Rectangular exit straight length: 150 mm.

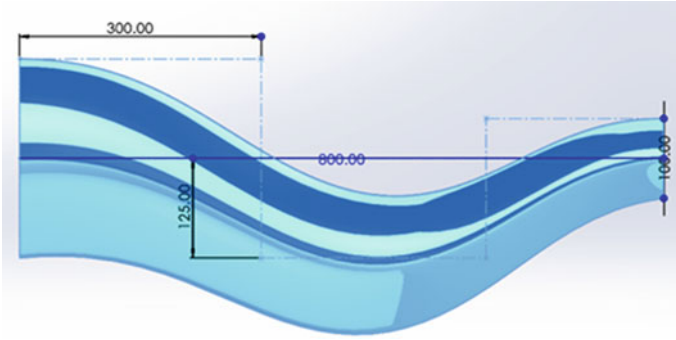


Fig. 1 Basic profile of the serpentine nozzle

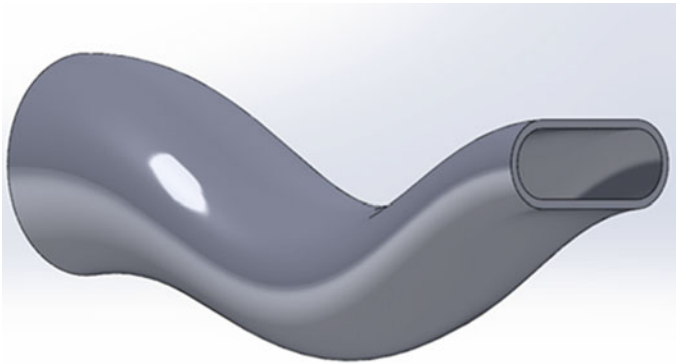


Fig. 2 Cambered rectangular exit

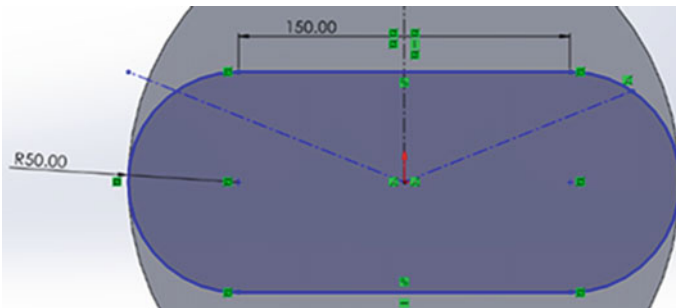


Fig. 3 Cambered rectangular exit cross-section

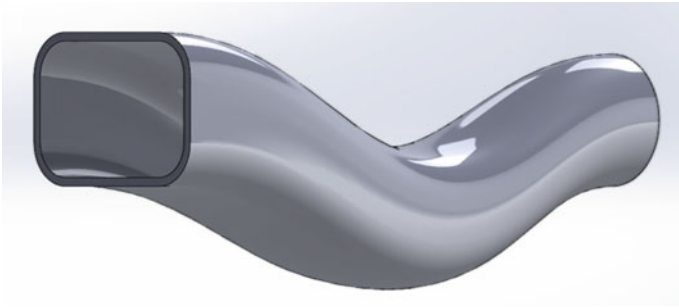


Fig. 4 Cambered rectangular exit

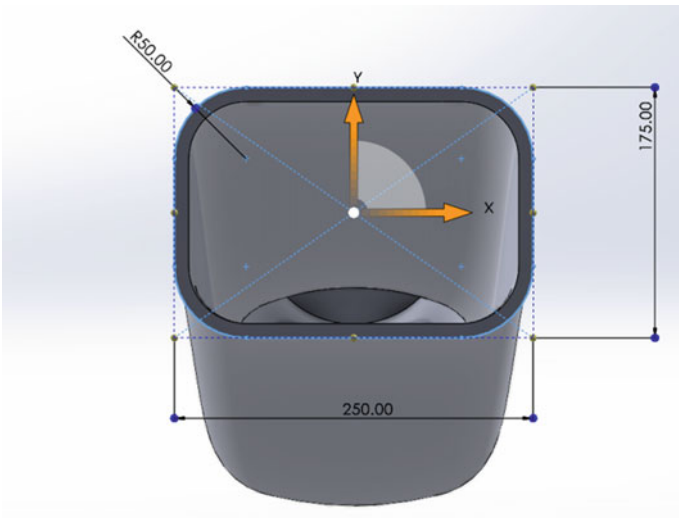


Fig. 5 Cambered rectangular exit cross-section

3.1.2 Cambered Rectangular Inlet

See Figs. 4 and 5

- Length of inlet: 250 mm.
- Breadth of inlet: 175 mm.
- Corner radius: 50 mm.
- Exit diameter: 150 mm.

3.1.3 Circular Inlet and Exit

See Fig. 6.

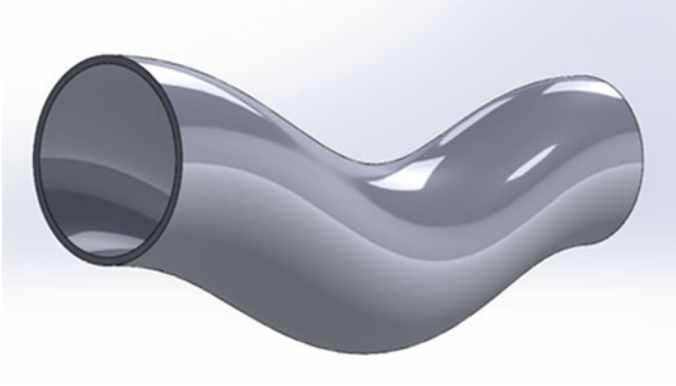


Fig. 6 Circular inlet and exit

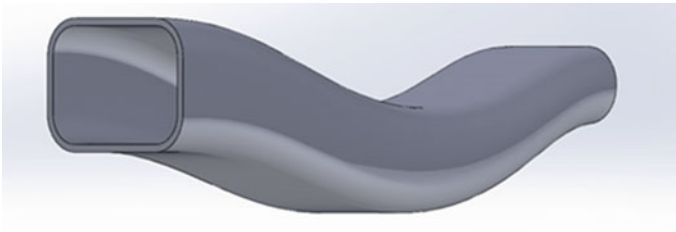


Fig. 7 Rectangular inlet and outlet

Circular inlet and exit.
 Inlet diameter: 250 mm.
 Exit diameter: 200 mm.

3.1.4 Rectangular Inlet and Exit

See Figs. 7 and 8.

- Same inlet as iteration 3.1.2.
- Same outlet as iteration 3.1.1.

3.2 Modeling and Meshing

In the CFD procedure, Unsteady Reynolds-Averaged Navier–Stokes (URANS) equations are used to simulate the flow. Since the nozzle is intended for subsonic flows, with a converging nozzle, as per the Rankine–Hugoniot conditions, there will be no flow separation inside the nozzle. This indicates that URANS equations will deliver

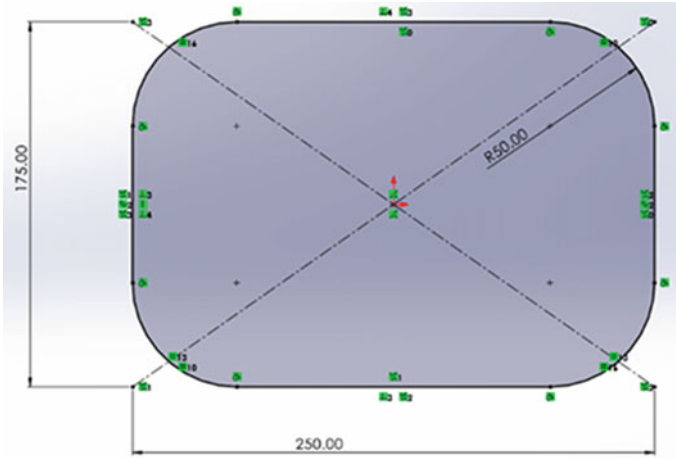


Fig. 8 Rectangular inlet cross-section

accurate results. For modeling the serpentine nozzle, the Realizable $k-\epsilon$ Turbulence Model is used. Due to high Reynolds numbers and high-pressure gradients, the standard $k-\epsilon$ Turbulence Model is not used as it cannot resolve boundary layer flow according to the law of the wall at higher pressure gradients. The equations governing the flow are as follows:

$$\frac{dk}{dt} = \frac{1}{\rho} \frac{\partial}{\partial x_j} \left(\frac{\mu_t \partial k}{\sigma_k \partial x_j} \right) + \frac{\mu_t}{\rho} \left(\frac{\partial U_i}{\partial x_j} + \frac{\partial U_j}{\partial x_i} \right) \frac{\partial U_i}{\partial x_j} - \epsilon, \tag{1}$$

$$\frac{d\epsilon}{dt} = \frac{1}{\rho} \frac{\partial}{\partial x_j} \left[\frac{\mu_t}{\sigma_\epsilon} \frac{\partial \epsilon}{\partial x_j} \right] + \frac{c_{\epsilon 1} \mu_t \epsilon}{\rho K} \left(\frac{\partial U_i}{\partial x_j} + \frac{\partial U_j}{\partial x_i} \right) \frac{\partial U_i}{\partial x_j} - c_{\epsilon 2} \frac{\epsilon^2}{k}. \tag{2}$$

The flow conditions are to be simulated at about Mach 0.9 at an altitude of 2000 m above mean sea level. The engine outlet parameters at this altitude are used as the boundary conditions. These have been derived from literature [1]. The boundary conditions are as follows:

- Inlet pressure: 1.25 MPa
- Inlet velocity: 299 m/s
- Inlet temperature: 1200 K
- Outlet pressure: 0 (Gauge)
- Outlet temperature: 290 K

Due to the complexity of the domain, Tet-Dominant meshing was preferred. A mesh independence study was conducted to study the effects of cell size and number on the flow. The coefficient of pressure at the core at $x/L = 0.5$ was chosen to be the control variable. The edge length was varied until a significant difference in

Table 1 Mesh metrics

Iteration	No. of cells	No. of nodes
Cambered rectangular exit	79,486	83,433
Cambered rectangular inlet	78,225	82,680
Circular inlet and exit	79,942	89,235
Rectangular inlet and exit	79,774	86,534

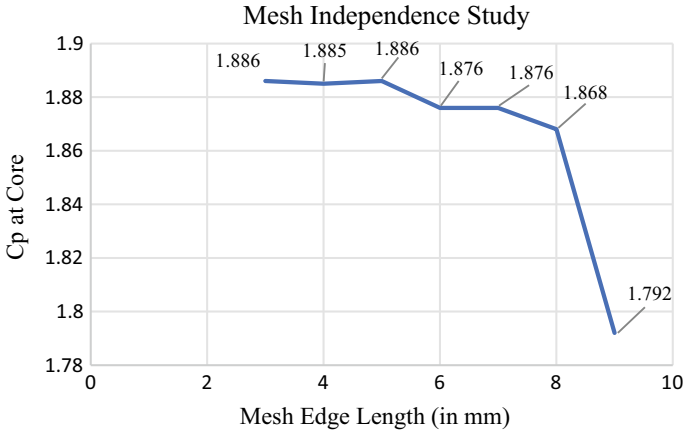


Fig. 9 Mesh independence study

the control variable was detected. The results of this mesh independence study are summarized in Table 1 (Fig. 9).

As per the study, the mesh with an edge length of 8 mm was the last mesh-independent solution. Meshing details and boundary conditions are given in Table 1.

- Tetrahedral meshing.
- Patch conformational.
- Average edge length: 8 mm.
- Inflation factor: 1.25.
- No. of inflation layers: 5.
- Transition ratios: 0.3.

3.3 Validation

Pressure values against the dimensionless length of the serpentine nozzle were plotted and compared with the CFD and wind tunnel testing data from the literature [1] as shown in Fig. 10.

Our CFD model shows remarkable similarity with the literature data, especially after 35% of the length. The maximum deviation from literature data is about 30%

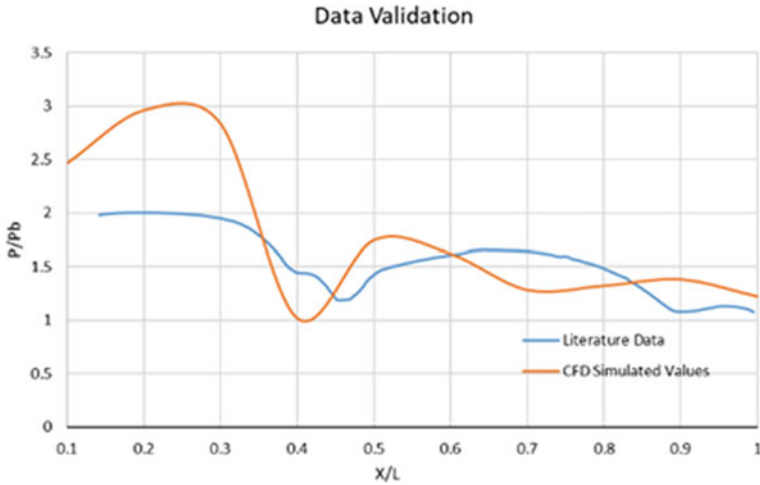


Fig. 10 Validation against literature data [1]

at x/L equals 0.25. This deviation at the beginning of the serpentine nozzle is inconsequential for this paper, as it focuses primarily on the effects near the exit of the nozzle, which is where the pressure distribution matters.

Furthermore, the CFD model accurately predicts the trend of the pressure changes throughout the serpentine nozzle, which is of primary importance for making qualitative decisions about optimal decisions.

4 Results and Discussion

Post-simulations, the obtained results for each of the four geometries have been summarized below:

4.1 Cambered Rectangular Exit

The pressure variation along the flow is observed in Fig. 11a. Static pressure drops after x/L 0.4 for the upper surface and x/L 0.6 for the lower surface. It can also be observed that the pressure drops from 2.36 to 0.4 bar at the exit.

Figure 11b exhibits that velocity starts picking up at 50% of the length. Velocity accelerates from about 300 m/s to almost 693 m/s, which is a significant increase in speed.

These two factors make this iteration a viable and preferred design for aircraft exhaust nozzles.

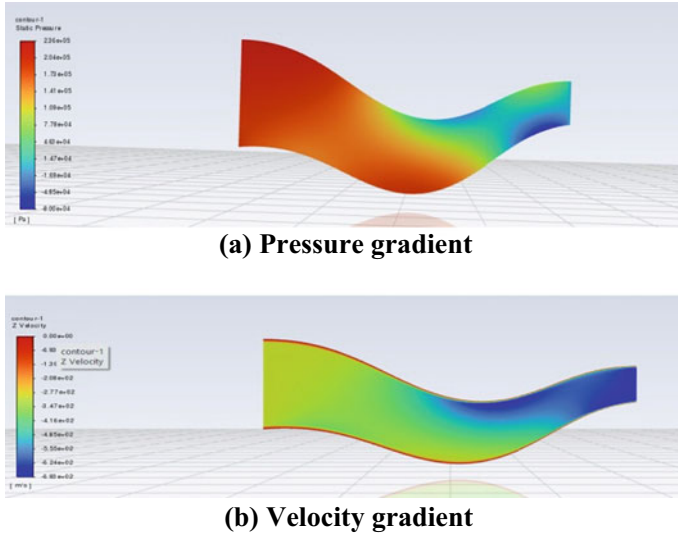


Fig. 11 a Pressure gradient. b Velocity gradient

4.2 Cambered Rectangular Inlet

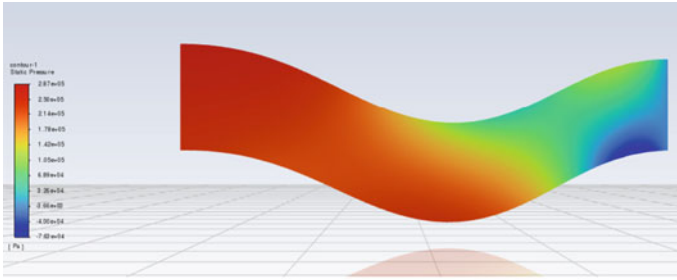
Figure 12a shows the static pressure field distribution along the central plane for the iteration. The contour shows that the pressure drops later if compared to the previous iteration. At the upper surface, the pressure drops at around $x/L = 0.5$ and $x/L = 0.8$ for the lower surface. Thus, expansion takes place later.

From Fig. 12b, it can be inferred that the final velocity at the nozzle exit is 766 m/s which is a significant expansion. It indicates that even though the expansion happens near the nozzle exit at $x/L = 0.6$, it occurs quite rapidly.

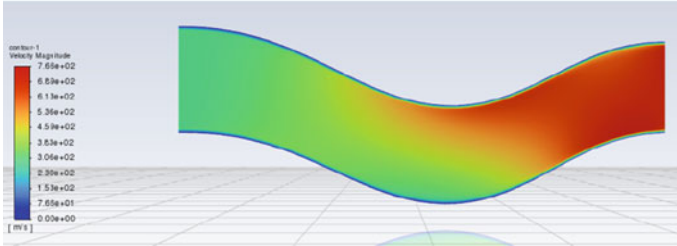
4.3 Pure Circular Exit

From Fig. 13a, it is evident that the peak pressure drop is encountered earlier in this iteration. However, the static pressure at the exit is higher than in the previous iteration. Pressure drop along the upper surface starts at $x/L = 0.35$, but the pressure drop across the lower surface starts at the same time.

Figure 13b indicates that the final velocity is smaller compared to the rectangular iteration at around 561 m/s, indicating that the expanding gasses have not been able to expand fully in the nozzle. This iteration is not ideal.

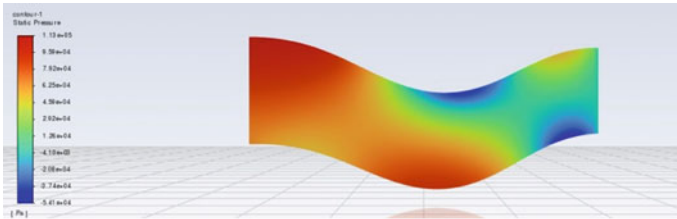


(a) Pressure gradient

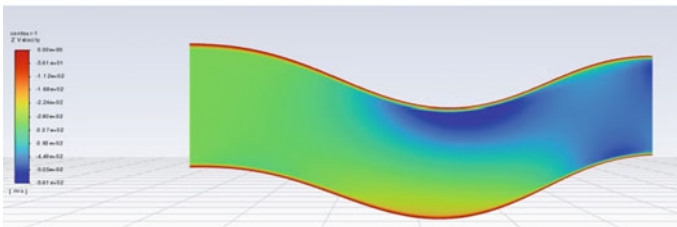


(b) Velocity gradient

Fig. 12 a Pressure gradient. b Velocity gradient



(a) Pressure gradient



(b) Velocity gradient

Fig. 13 a Pressure gradient. b Velocity gradient

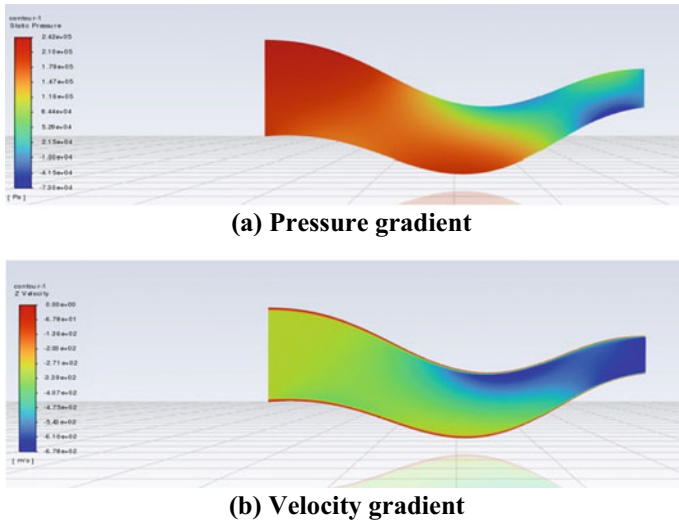


Fig. 14 a Pressure gradient. b Velocity gradient

4.4 Pure Rectangular Exit

From Fig. 14a, inferences indicate that the magnitude of static pressure drop is the least in this iteration, from 2.4 bar to 0.2 bar. The pressure characteristics for both surfaces are similar to the cambered rectangular iteration.

Figure 14b indicates that freestream velocity picks up quite late, at around 80% of the cavity length. There is a significant flow acceleration, from 300 m/s to about 678 m/s, indicating good acceleration.

The results obtained from these simulations allow us to plot the velocity ratio as a function of the area ratio for serpentine nozzles, as seen in Fig. 15.

From Fig. 15, we find a quadratic relation between the area and velocity ratios. The graph further highlights that the increase in area ratio does not keep up with the increase in velocity ratio.

5 Conclusions

From the present computational investigation, the following conclusions are drawn:

- Rectangular inlets and circular outlets give the best flow characteristics.
- Significant velocity increase and the pressure penalty are also lower when compared to other inlet outlet conditions investigated.
- It follows that a smaller exit area leads to a velocity increase but results in unfavorable pressure characteristics.

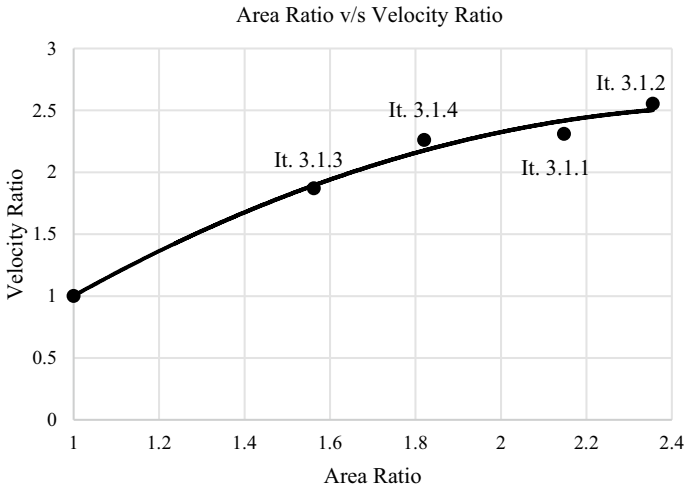


Fig. 15 Area ratio versus velocity ratio

- Increasing the area ratio from 1.56 to 1.82 (~16% increase) leads to an 18% increase in the velocity.
- Increasing the area ratio further does not lead to proportionate velocity gains. Increasing the area ratio from 1.82 to 2.15 (~18% increase) leads to only a 2% increase in the velocity ratio.
- Similarly, increasing the area ratio from 1.82 to 2.35 (~29% increase) leads to only a 13% increase in the velocity ratio.

Acknowledgements The authors would like to thank Mr. Aditya Shah, Mr. Sudhanva Rao Santhur, and Dr.Ramola Sinha for their support.

Nomenclature

C_p	Pressure coefficient (-)
OASPL	Overall sound pressure level (dB)
x	Distance from the nozzle inlet (m)
L	Length of the serpentine nozzle (m)
M_∞	Free stream Mach No. (-)
P	Static pressure (Pa)
P_b	Back pressure (Pa)
AMSL	Above mean sea level (m)
σ	Wall stress (Pa)
K	Turbulent kinetic energy (m^2/s^2)
ε	Rate of dissipation of TKE (m^2/s^3)

μ	Kinematic viscosity (cm/s ²)
u_i	Relative velocity (in direction) (m/s)
$c_{\varepsilon 1}, c_{\varepsilon 2}$	Closure coefficients (–)

References

1. Hui Z, Shi J, Zhou L, Wang Z, Liu Y (2021) Experimental investigation of serpentine nozzles for turbofan. Shaanxi Key Laboratory of Internal Aerodynamics in Aero-Engine, School of Power and Energy, Northwestern Polytechnical University, 710072, Xi'an, People's Republic of China
2. Cheng W, Wang Z, Zhou L, Sun X, Shi J (2019) Investigation of infrared signature of serpentine nozzle for turbofan. *J Thermophys Heat Transf* 33(1):170–178
3. Shan Y, Zhou X, Tan X, Zhang J, Wu Y (2019) Parametric design method and performance analysis of double S-shaped nozzles. *Int J Aerosp Eng* 2019:24 Article ID 4694837. <https://doi.org/10.1155/2019/4694837>
4. Nageswara Rao A, Arora R, Kushari A High subsonic flow field from the serpentine nozzle. In: 8th international conference on fluid flow, heat and mass transfer (FFHMT'21). <https://doi.org/10.11159/ffhmt21.144>
5. Sun X, Wang Z, Zhou L, Shi J, Liu Z (2015) Experimental and computational investigation of double serpentine nozzle. *Proc Inst Mech Eng Part G J Aerosp Eng*. 229(11):2035–2050. <https://doi.org/10.1177/0954410014564402>
6. Da X, Fan J (2020) Closed-loop flow control of an ultra-compact serpentine inlet based on non-dimensional model. *Chin J Aeronaut* 33(10):2555–2562. ISSN 1000-9361